Running title: Impacts of the MJO on Winter Rainfall in China

Impacts of the MJO on Winter Rainfall and Circulation in China

Jia Xiaolong[1*] (贾小龙), Chen Lijuan[1] (陈丽娟), Ren Fumin[1] (任福民), and Li Chongyin[2, 3] (李崇银)

[1]*National Climate Center, China Meteorological Administration, Beijing* 100081

[2]*State Key Laboratory of Numerical Modeling for Atmospheric Sciences and Geophysical Fluid Dynamics (LASG), Institute of Atmospheric Physics, Chinese Academy of Sciences, Beijing* 100029

[3]*Institute of Meteorology, PLA University of Science and Technology, Nanjing* 211101

(Received 12 March 1020; revised 12 July 2010)

ABSTRACT

Impacts of the MJO on winter rainfall and circulation in China are investigated using a real-time multivariate MJO index. Composite results using the daily rainfall anomalies and "rainy day" anomalies according to eight different MJO phases show that the MJO has considerable influence on winter rainfall in China. Rainfall anomalies show systematic and substantial changes (enhanced/suppressed) in the Yangtze River Basin and South China with the eastward propagation of the MJO convective center from the Indian Ocean to the western Pacific. When the MJO is in phase 2 and 3 (MJO convective center is located over the Indian Ocean), rainfall probability is significantly enhanced. While in phase 6 and 7 (MJO convective center is over the western Pacific), rainfall probability is significantly reduced.

MJO in winter influences the rainfall in China mainly through modulating the circulation in the subtropics and mid-high latitudes. For the subtropics, MJO influences the northward moisture transport coming from the Bay of Bengal and the

[*]Corresponding author: Jia Xiaolong, jiaxl@cma.gov.cn

South China Sea by modulating the southern trough of the Bay of Bengal and the western Pacific subtropical high. For the mid-high latitudes, the propagation of the low frequency perturbations associated with the eastward-propagating MJO convection modulate the circulation in the mid-high latitudes, e.g. the East Asian winter monsoon and the low trough over central Asia.

Key words: MJO, rainfall anomaly, subtropics, mid-high latitudes, vertical motion

Citation: Jia, X., L. Chen, F. Ren, and C. Li, 2010: Impacts of the MJO on winter rainfall and circulation in China. *Adv. Atmos. Sci.*, doi: 10.1007/s00376-010-9118-z.

1. Introduction

The major mode of intraseasonal variability in the tropical atmosphere is the MJO (Madden and Julian, 1971, 1972). Characteristics of this oscillation have been well documented in many observational studies (e.g. Lau and Chan, 1985; Knuston and Weickmann, 1987; Li, 1990; Hendon and Salby, 1994; Madden and Julian, 1994; Salby and Hendon, 1994; Jones and Wear, 1996; Maloney and Hartmann, 1998; Woolnough et al., 2000; Sperber, 2004; and for a recent review see Zhang, 2005). In short, the MJO is characterized by its planetary scale of wavenumbers 1–3 and its eastward propagation with a period of approximately 30–60 days. This oscillation also has an evident seasonality, with larger amplitude during boreal winter and spring than summer. This oscillation also shows a baroclinic structure in the vertical, with its zonal wind anomalies in the lower and upper troposphere being out phase with each other. The MJO convection over the Indian and western Pacific Ocean is strongly coupled to the circulation as a mixed Kelvin-Rossby wave and propagates slowly eastward (e.g. Rui and Wang, 1990; Chao and Lin, 1994). Away from the convective region of the western Pacific, the oscillation is characterized by a Kelvin wave with more rapid eastward propagation (e.g. Sperber, 2004).

The importance of the MJO to tropical and global weather and climate has become increasingly apparent. The direct impacts of the MJO on tropical weather and climate

phenomena have been widely documented. For instance, the MJO can influence the onset of and breaks in the summer monsoons over Asia (e.g. Lau and Chan, 1986; Mu and Li, 2000; Lawrence and Webster, 2002), Australia (e.g. Hendon and Liebmann, 1990; Wheeler and McBride, 2005), America (e.g. Paegle et al., 2000; Higgins and Shi, 2001), and Africa (e.g. Matthews, 2004). It also significantly modulates tropical cyclone activities (e.g. Maloney and Hartmann, 2000; Ho et al., 2006). The evolution of the ENSO can also be affected by the MJO (e.g. Lau and Shen, 1988; Li and Zhou, 1994; Kessler et al., 1995; Li and Long, 2002; Zhang and Gottschalck, 2002). However, the influence of the MJO on weather and climate is not only confined to the tropics. It can also significantly modulate variations in weather and climate in the far-reaching subtropics and midlatitudes (e.g. Jones, 2000; Bond and Vecchi, 2003; Carvalho et al., 2004; Barlow et al., 2005; Donald et al., 2006; Wheeler and Hendon, 2008; Jeong et al., 2008; Zhang et al., 2008).

Wheeler and Hendon (2004) designed a real-time multivariate MJO index (RMM), which provides real-time MJO information, including its strength and position. This index has been used in MJO monitoring and diagnostic operation in several operational administrations, e.g. the Australia Meteorology Bureau and the Climate Prediction Center/National Centers for Environmental Prediction (CPC/NCEP). Using this index, much work has been done to study the impact of the MJO on weather and climate anomalies in different areas (e.g. Wheeler and Hendon, 2004; Donald et al., 2006; Wheeler and Hendon, 2009; Jeong et al., 2008; Zhang et al., 2008). Recently, using the Wheeler and Hendon MJO index, Zhang et al. (2009) studied the impact of the MJO on summer rainfall anomalies in Southeast China.

China is mainly located in the subtropics and midlatitudes, but the tropical circulation system, including the tropical intraseasonal oscillation, plays important roles in weather/climate anomalies in China. However, most studies have focused on intraseasonal oscillations over specific areas, e.g. South China, the South China Sea, or the western Pacific warm pool, or on summertime, and, especially, on the meridional propagation of intraseasonal oscillation (e.g. Chen et al., 2001; Yang and Li, 2003; Ju and Zhao, 2005; Xu and Zhu, 2004). Relatively little work has been

carried out regarding the MJO as a global scale circulation system to study the impact of its zonal propagation on wintertime weather and climate anomalies in China. Owing to the fact that the MJO is mainly a propagating mode in the tropics, and studies have indicated that the extratropical circulation response to diabatic heating associated with tropical convection is dependent not only on the background mean flow, but on the magnitude, position, and time evolution of the diabatic forcing (e.g. Ting and Sardeshmukh, 1993; Jin and Hoskins, 1995; Bladé and Hartmann, 1995), it would therefore be interesting to investigate the impact of the spatiotemporal evolution of the MJO to rainfall in China.

In winter, the Chinese mainland is dominated mainly by a strong winter monsoon system, which produces prevailing northwesterly and northeasterly winds in the lower troposphere carrying cold and dry air. Consequently, in winter, rainfall amounts over the mainland are limited relative to those in other seasons; whereas, the anomalies can also produce severe disasters, as demonstrated by the unprecedented freezing and snow disasters which occurred in the winter of 2007/2008 in China (e.g. Wang et al., 2008; Gao et al., 2008). Considering the seasonality of the MJO with the largest strength in winter and using the Wheeler and Hendon MJO index (2004), this paper will investigate the impact of the MJO on winter rainfall anomalies in China, as well as analyze the possible mechanism by diagnosing the corresponding large-scale circulation and the physical fields associated with the MJO.

The remainder of the paper is organized as follows. Descriptions of the data and analysis method used are presented in section 2. In section 3, the variation of winter rainfall with respect to the MJO is explored. The corresponding large-scale circulation anomalies and physical fields affected by the MJO are further investigated in section 4. Finally, a summary and conclusions are presented in section 5.

2. Data and methods

2.1 *Data*

2.1.1 *The MJO index*

The MJO index used was a real-time multivariate MJO (RMM) index developed by

Wheeler and Hendon (2004), downloaded from the website of the Australia Meteorological Bureau (http://www.bom.gov.au/bmrc/clfor/cfstaff/matw/maproom/RMM/). This index defines the MJO through projection of daily anomaly data onto the leading pair of empirical orthogonal functions (EOFs) of combined fields of equatorially-averaged (15°S–15°N) Outgoing Longwave Radiation (OLR), 850 hPa zonal wind, and 200 hPa zonal wind, to obtain two principal component time series (called RMM1 and RMM2). Longer-timescale variability resulting from ENSO and other interannual variations with a period longer than about 200 days is removed prior to this projection; no temporal filtering is applied. Despite using no intraseasonal time filtering, the index strongly discriminates the 30–80 day MJO signals.

The RMM1 and RMM2 index defines a 2D phase space. In this phase space, the eastward propagation of the MJO can be categorized into eight phases, each corresponding to the geographical position of its active convective center (Fig. 1). According to the magnitude and propagation of the RMM index, strong MJO can be defined when $\sqrt{RMM1^2 + RMM2^2} \geq 1$, and weak MJO when $\sqrt{RMM1^2 + RMM2^2} < 1$. Therefore, in the 2D phase space diagram, strong MJO events appear as large anti-clockwise excursions about the origin, and weak MJO usually appears as somewhat random movement near the origin. These phases make up a full MJO cycle originating from the western Indian Ocean and decaying over the central Pacific. For instance, phases 1 and 2 mark the time when the MJO's convective envelopes are centered near the western Indian Ocean and phases 7 and 8 mark the time when it is near the dateline in the Pacific. The MJO index data used here is for 1 January 1975 to 31 December 2006.

2.1.2 *Rainfall and circulation data*

Daily rainfall data used were from 545 stations in China covering the period of 1975–2006, collected and compiled by the National Meteorological Information Center of the China Meteorological Administration (CMA). Some of the data from these stations for the period 1975-2006 were missing. Most of the stations are located

in the eastern region of China (Fig. 2). In addition, NCEP–NCAR daily reanalysis data(Kalney,1996), including sea level pressure (SLP), wind, vertical velocity, specific humidity, and geopotential height covering the period of 1 January 1975 31 December 2006 were also used.

2.2 *Methods*

Daily anomalies of rainfall and other variables were calculated by subtracting their climatological means from the original data. Composites of mean daily anomalies were computed for each of the eight phases of the MJO according to the RMM index with the same MJO phases in boreal winter during 1975–2006. Winter in this paper is defined as the period from December to February. We also generated composites for "rainy days", which was done with total rainfall data by counting the number of days at each station for each composite MJO phase for which the daily rainfall was greater than 0.1 mm.

Statistical significance for the composites was judged using a local *t*-test applied to the difference between two sample means. For horizontal wind, vertical velocity, SLP, geopotential height, and moisture flux, which are normally distributed, the composites were estimated to be significantly different from zero at the 95% level. The formula is

$$t=\frac{\left|\sum_{i=1}^{N} F'/N\right|}{\sigma\sqrt{1/N'}}, \tag{1}$$

where $\sum F'/N$ is the anomaly field composite for different MJO phase categories, σ is the daily standard deviation of F' in winter, and N' is the effective sample size approximation by $N'\cong N\frac{1-\rho}{1+\rho}$ (Wilks, 2006), N is the number of days in each MJO phase, and ρ is the lag-1 autocorrelation coefficient of F′ in winter.

Rainfall has a very skewed probability distribution and so a direct *t*-test is not valid. Therefore, before the *t*-test was used, we first transformed the original daily rainfall

data to make them less skewed. Since there are lots of zeros in daily rainfall data, the traditional Box-Cox method which requires the data to be positive is not applicable. Instead, we adopted the method introduced by Yeo and Johnson (2000), which can transform the zero and negative data directly. The transformation is

$$\begin{cases} \dfrac{(x+1)^{\lambda}-1}{\lambda}, x \geq 0 \\ \dfrac{-\left\{(-x+1)^{2-\lambda}-1\right\}}{2-\lambda}, x < 0 \end{cases}, \quad (2)$$

where λ is set to be the best theoretical value 0.555. After the transformation, the data have an approximate normal distribution and the *t*-test can be used.

3. Variation in winter rainfall anomalies related to the MJO in China

Firstly, it is necessary to give the standard deviation of daily rainfall in winter in China. As shown in Fig. 3, the largest variation in daily rainfall in winter occurs in the Yangtze River Basin and South China, with the maximum standard deviation exceeding 6 mm d^{-1}, while variation to the north of the Yangtze River is smaller, relatively. Therefore, we focus on rainfall variations in the Yangtze River Basin and South China in this paper. Figure 4 displays composites of daily rainfall anomalies for the eight strong MJO phases. It is very clear that winter rainfall anomalies in China show systemic variations when the MJO propagates from the Indian Ocean into the western Pacific. Winter rainfall over the Yangtze River Basin and South China are greater than normal when the MJO is in phase 2 and phase 3 (the MJO convective center is located over the Indian Ocean), with the maximum anomalies exceeding 2 mm d^{-1}, which is close to the climatological mean, and then positive anomalies weaken and shift southward as phases 4 and 5 show. When the MJO is in phases 6–8, especially in phases 6 and phase 7 (the MJO convective center is located over the Western Pacific), rainfall over the majority of Yangtze River Basin and South China are less than normal, with the maximum negative anomalies exceeding -1.2 mm d^{-1}, which is about 50% relative to the climatologic mean.

Owing to the fact that winter rainfall amounts are much less in North China than

South China, Fig. 4 mainly reflects differences in rainfall amount anomalies in South China among different MJO phases. Figure 5 shows composite “rainy day” anomalies in each MJO phase. Similar results to Fig. 4 can be seen in that when the MJO is in phases 2 and 3, rainfall probability is significantly enhanced in the majority of regions in the Yangtze River Basin and South China, with the maximum exceeding 16 days, which is about 70% greater than the climatological mean. In phases 6 – 8, meanwhile, the rainfall probability is significantly reduced in the majority of regions, with the maximum exceeding -8 days, which is about 40% less than normal in some regions.

If one takes the Yangtze River Basin and South China as a regional mean, variation in rainfall anomalies accompanying the transition of the MJO convective phase can be seen clearly in Fig. 6. Figure 6 displays averaged daily rainfall anomalies and the departure percentage relative to the climatological mean for those stations located in regions east of 105°E and south of 32.5°N. The regional mean rainfall anomalies in the composites are all positive in phases 1–5 and negative in phases 6–8, however the variation is also most significant in phases 2 and 3, and phases 6 and 7. The average positive rainfall anomaly is 0.65 mm d^{-1} in phase 2 and the average negative anomaly in phase 6 is -0.4 mm d^{-1}, which amounts to almost 45% and 30% relative to the climatological mean, respectively.

In a word, winter rainfall anomalies show systemic variation associated with the evolution of the MJO. The most significant variation was found to occur in phases 2 and 3, and phases 6 and 7. When the MJO convective center is located over the Indian Ocean (western Pacific) the probability of rainfall over major regions of China is significantly enhanced (reduced).

4. Large scale circulation and physical fields associated with the MJO

The MJO is a dominant mode in the tropics, but China is mainly located in the far-reaching subtropical and midlatitude regions. Given this, how does the MJO influence variation in rainfall anomalies in China? The answer to this can be gained partly by investigating the evolution of MJO-related large-scale circulation anomalies.

4.1 *Tropical and subtropical moisture transport*

The influence of the MJO on circulations is more robust in the tropics and subtropics, and, as we know, moisture transport plays a key role in rainfall. In winter, moisture supply to the Chinese mainland comes mainly from the tropics or subtropics, e.g. the Bay of the Bengal and the South China Sea/western Pacific. Therefore, firstly, it is necessary to investigate moisture transport when the MJO propagates into different phases. Figure 7 gives the composite anomalies of moisture flux integrated from 1000 – 300 hPa for the eight MJO phases. It can be seen that in phases 2 – 3, northward moisture transport to mainland China coming from the Bay of the Bengal and the South China Sea is strengthened and carries more moisture to South China. The largest water vapor convergence occurs just in the Yangtze River Basin and South China; whereas, the Bay of the Bengal and the South China Sea is the moisture source (divergence). When the MJO propagates eastward, the northward moisture transport band also retreats southward, which is why positive rainfall anomalies in South China also show a continuous variation of retreating southward from phase 2 – 5, as shown in Figs. 4 and 5. When the MJO propagates into the western Pacific (phases 6 and 7), moisture transport into South China is southward, and the Yangtze River Basin and South China are also mainly dominated by anomalous moisture divergence, which indicates that the northward moisture transport into China coming from the Bay of the Bengal and the South China Sea is suppressed. The southern trough of the Bay of the Bengal and the western Pacific subtropical high are major contributors to the anomalous moisture transport.

Figure 8 further displays the variation in the southern trough of the Bay of Bengal for the eight MJO phases. One can see that it shows a continuous variation from strong to weak as the MJO propagates from the Indian Ocean to the western Pacific. The most significant variation is between phases 2 and 3, and phases 6–8. In phases 2 and 3, the southern trough of the Bay of Bengal is much deeper, and therefore favors moisture transportation northward into South China. In phases 6–8, it is much weaker than normal. Besides the southern trough of the Bay of Bengal, the moisture from the South China Sea transported by southwesterly airflows along the west side of the

western Pacific subtropical high also plays an important role in winter rainfall in China. For brevity, Fig. 9 gives the contour of 5870 gpm at 500 hPa for MJO phases 2 and 6. It is clear that the western Pacific subtropical high is farther westward with the western ridge of the 5870 line reaching near 113°E for MJO phase 2, while for phase 6, it is near 133°E. Obviously, in phase 2, the moisture coming from the South China Sea may be more easily transported to the Chinese mainland by the southwesterly airflows over the west of the western Pacific subtropical high than in phase 6.

4.2 *Mid-high latitude circulation*

Many studies have suggested that the influence of the MJO on atmospheric circulation is not only confined to the tropics and subtropics, but that it can also significantly modulate variations in the far-reaching mid-high latitudes by teleconnection (Bond and Vecchi, 2003; Carvalho et al., 2004; Barlow et al., 2005; Donald et al., 2006; Wheeler and Hendon, 2008; Zhang et al., 2008). Figure 10 displays geopotential height at 500 hPa for the eight MJO phases. It is clear that circulation anomalies in the midlatitudes also propagate eastward, accompanying the MJO's eastward propagation. Here, we focus mainly on its impacts on circulation anomalies over East Asia. It can be seen that when the MJO is in phase 1, East Asia is dominated entirely by positive height anomalies, with the anomaly center over neighboring Korea. When the MJO propagates into phases 2 and 3, the positive anomaly center moves eastward to over the sea, and the East Asian mainland is basically controlled by negative anomalies, with the anomaly center over Mongolia. In addition, it is noticeable that Central Asia is also dominated by negative anomalies and that the Urals are controlled by a strong positive anomaly center in phase 2. Therefore, the propagation of midlatitude low-frequency perturbations results in a "western-low–eastern-high" pattern over East Asia and a "western-high–eastern -low" pattern over the Eurasian mainland in MJO phase 2. This kind of anomalous circulation pattern indicates the development of a Urals blocking high and a low trough over Central Asia, which is in favor of the invasion of cold air from the high latitudes into mainland China from the west and north. Meanwhile, the

“western-high–eastern-low” pattern over East Asia indicates a weak Baikal ridge and East Asia major trough, two major systems over the westerly mean flows in winter over East Asia, which result in a weak East Asian winter monsoon along the coast of the East Asian mainland.

In the following phases (phases 4 and 5), circulation anomalies over East Asia are much weaker relative to phases 2 and 3. When the MJO moves into phases 6 and 7 (MJO convective center is over the western Pacific), the anomalous circulation pattern over East Asia is a “western-high–eastern-low” distribution, which is almost opposite to phases 2 and 3. Mainland China is dominated by positive geopotential height anomalies, but meanwhile, in this circulation pattern, the East Asian coast is dominated by anomalous northerlies, which indicate a strong winter monsoon and a strong winter monsoon flow across East China, which is not favorable for the convergence of warm-wet and cold-dry airs over East China. Meanwhile, anomalous northerlies control the South China Sea and the Bay of Bengal, indicating weak moisture transport northward, as shown in Fig. 7. Figure 11 further shows variations of the low trough over Central Asia a contributor of cold air for the eight MJO phases. One can see that it displays a continuous variation from strong to weak as the MJO propagates from the Indian Ocean to the western Pacific. The most significant variation is between phases 2 and 3, and phases 6–8. In phases 2 and 3, the low trough over Central Asia is much deeper, in favor of cold air activities. In phases 6–8, it is much weaker than normal.

Propagation of low frequency perturbations in the midlatitudes shown in Fig. 11 is also reflected in the lower troposphere. Figure 12 shows the SLP and 850 hPa wind anomalies for the eight MJO phases. The SLP anomalies in the midlatitudes also show significant variation. For instance, SLP anomalies also propagate eastward with centers near 40–45°N, corresponding to two components of East Asian winter monsoon systems: the Mongolia high and Aleutian low. Consequently, this would modulate the state of the East Asian winter monsoon. For instance, in MJO phases 2 and 3, SLP anomalies over the sea to the East Asian mainland is positive, indicating a weaker than average Aleutian Low, and this, with the negative anomalies dominating

southern Asia, leads to the anomalous southerly along the coast of the East Asian mainland, indicating a weak winter monsoon influencing China. Additionally, we can also see that northern Asia has positive anomalies, indicating active cold air activities appearing at some higher latitudes (north of 40°N), which is favorable for convergence between the southerly and northerly over eastern China. When the MJO convection is over the western Pacific (phases 6 and 7), the East Asian mainland is controlled by positive SLP anomalies, and the sea to East Asia is dominated by negative SLP anomalies. This leads to northerly anomalies traversing the whole East Asian coast, even into the South China Sea. In this case, the East Asian mainland is controlled mainly by dry-cold air coming from high latitudes, brought by too strong an East Asian winter monsoon, which is not favorable for the delivery of more rainfall than normal in China. In order to further explore variations in the East Asian winter monsoon relating to the propagation of the MJO, we calculated an East Asian winter monsoon index designed by Chen et al. (2000), which is constructed as the 1000 hPa meridional wind averaged within the region (10–25°N, 110–130°E) and (25–40°N, 120–140°E). Figure 13 shows values of this index in the eight MJO phases. Positive (negative) values indicate a weak (strong) winter monsoon. It is clear that the East Asian winter monsoon displays obvious changes from strong to weak when the MJO propagates from the Indian Ocean to the western Pacific.

4.3 *Vertical motions*

Figure 14 displays vertical velocity anomalies and meridional-vertical wind anomalies averaged between 110–120°E for the eight MJO phases. It can be seen that anomalous ascending motion dominates near 20–30°N in MJO phases 2 and 3, which, without doubt, favors more precipitation. Additionally, there is also a descending branch close to 30°N, especially in phase 2, and this, with the anomalous ascending motion over 30°N, forms an anomalous meridional circulation contributing to southerly anomalies at low levels. For MJO phases 6–8, anomalous descending motions dominate the Chinese mainland, which is not favorable for more precipitation, especially when the MJO convection moves into the western Pacific (phase 6) and the

anomalous meridional circulation near 110 – 120°E, with ascending motion over regions between the equator and 10°N and a descending branch over the Chinese mainland, is obvious, which contributes to the low-level northerly anomalies.

5. Summary and conclusions

This study investigated the impacts of the MJO on winter rainfall and circulation in China using the RMM index designed by Wheeler and Hendon (2004). Composite results using daily rainfall anomalies and "rainy day" anomalies according to the eight different MJO phases showed that the MJO has considerable influence on winter rainfall anomalies in China. Rainfall anomalies showed systematic and substantial changes (enhanced/suppressed) in China, particularly in southern China, with the eastward propagation of the MJO convective center from the Indian Ocean to the western Pacific. The largest variation appeared between phases 2 and 3 (MJO convective center was over the Indian Ocean) and phases 6 and 7 (MJO convective center was over the western Pacific). Regional mean rainfall increased by about 45% in phase 2 and decreased by 30% in phase 6, relative to the climatological mean.

Large-scale circulation and physical fields associated with the MJO were further explored to explain the linkage between the MJO and rainfall variations in winter in China. It was found that the MJO can influence winter rainfall in China by direct impacts and remote correlation, which can be realized by circulation anomalies in the subtropics and mid-high latitudes, respectively.

For the subtropics, the MJO was found to influence the northward moisture transport coming from the Bay of Bengal and the South China Sea by modulating the southern trough of the Bay of Bengal and the western Pacific subtropical high, two major contributors to moisture transport. When the MJO was in phases 2 and 3, the southern trough of the Bay of Bengal was enhanced and the western Pacific subtropical high was located farther westward and also enhanced; therefore, the northward moisture transport onto the Chinese mainland was strengthened, and the largest water vapor convergence occurred just over the Yangtze River Basin and South China. In phases 6 and 7, meanwhile, these two subtropical systems were both

weakened.

For the mid-high latitudes, the propagation of low frequency perturbations in the midlatitudes accompanying the eastward-propagating MJO modulated the circulation in the mid-high latitudes, particularly the East Asian winter monsoon. When in MJO phases 2 and 3, the propagation of mid-high perturbations resulted in a "western-low–eastern-high" pattern over East Asia, indicating the development of a low trough over Central Asia, which was favorable for the invasion of cold air from the high latitudes onto the Chinese mainland from the west and northwest, and the weak Baikal ridge and East Asia major trough, which resulted in a weak East Asian winter monsoon along the coast of the East Asian mainland. A weak winter monsoon was also favorable to warm and moist air coming from the lower latitudes, transporting northward and converging with cold air coming from the high latitudes, which led to a strong ascending motion over the Yangtze River Basin and South China. In MJO phases 6 and 7, the East Asian winter monsoon was strengthened, which led to eastern China being dominated by strong and dry-cold northerlies with limited moisture.

Acknowledgments. This research was supported by the National Natural Science Foundation of China (40905035), the 973 Science Foundation of China (2010CB428606, 2006CB403600), the Science Foundation of China (U0833602), the National Department Public Benefit Research Foundation of China (GYHY200806004, GYHY200906015) and the Key Technologies R&D Program of China under grant nos. 2007BAC29B04 and 2009BAC51B00.

REFERENCES

Barlow, M., M. Wheeler, B. Lyon, and H. Cullen, 2005: Modulation of daily precipitation over southwest Asia by the Madden-Julian oscillation. *Mon. Wea. Rev*., **133**, 3579-3594.

Blade, I., and D. L. Hartmann, 1995: The linear and nonlinear extratropical response of the atmosphere to tropical intraseasonal heating. *J. Atmos. Sci.*, **52**, 4448-4471.

Bond, N. A., and G. A. Vecchi, 2003: The influence of the Madden–Julian oscillation on precipitation in Oregon and Washington. *Wea. Forecast*, **18**, 600–613.

Carvalho, L. M., C. Jones, and B. Liebmann, 2004: The South Atlantic convergence zone: Intensity, form, persistence, and relationships with intraseasonal to interannual activity and extreme rainfall. *J. Climate*, **17**, 88-108.

Chao, W. C., and S. J. Lin. 1994: Tropical intraseasonal oscillation, supper cloud cluster, and cumulus convection schemes. *J. Atmos. Sci*., **51**, 1282-1297.

Chen, L. X., C. W. Zhu, W. Wang, and P. Q. Zhang, 2001: Analysis of the Characteristics of 30-60 Day Low-Frequency Oscillation over Asia during 1998 SCSMEX. *Adv. Atmos. Sc.i*, **18**(4), 623-638.

Chen, W., F. G. Hans, and R. H. Huang, 2000: The interannual variability of East Asia winter monsoon and its relation to the summer monsoon. *Adv. Atmos. Sci.,* **17**, (1), 48-60.

Donald, A., H. Meinke, B. Power, A. H. N. Maia, M. C. Wheeler, N. White, R. C. Stone, and J. Ribbe, 2006: Near-global impact of the Madden-Julian oscillation on rainfall. *Geophys. Res. Lett*., **33**, L09704, doi: 10.1029/2005 GL0 25155.

Gao, H, and Coauthors, 2008: Analysis of the severe cold surge, ice-snow and frozen disasters in south China during January 2008: II. Possible climatic causes. *Meteorological Monthly*, **34**(4), 101-106. (in Chinese)

Hendon, H. H., and B. Liebmann, 1990: The intraseasonal (30-50 day) oscillation of the Australian summer monsoon. *J. Atmos. Sci.,* **47**, 2909-2924.

Hendon, H. H, and M. L. Salby, 1994: The life cycle of the Madden-Julian oscillation. *J. Atmos. Sci.*, **51**, 2225-2237.

Higgins, R. W., and W. Shi, 2001: Intercomparison of the principal modes of interannual and intraseasonal variability of the North American Monsoon System. *J. Climate*, **14**, 403-417.

Variation of tropical cyclone activity in the South Indian Ocean: El Niño–Southern Oscillation and Madden-Julian Oscillation effects

Ho, C. H., J. H. Kim, J. H. Jeong, H. S. Kim, and D. L. Chen, 2006: Variation of tropical cyclone activity in the South Indian Ocean: El Niño–Southern

Oscillation and Madden-Julian Oscillation effects. *J. Geophys. Res.*, **111**, D22101, doi:10.1029/2006JD007289.

Jeong, J. H., B. M. Kim, C. H. Ho, and Y. Noh, 2008: Systematic variation in wintertime precipitation in East Asia by MJO-induced extratropical vertical motion. *J. Climate*, **21**,788-801.

Jin, F., and B. J. Hoskins, 1995: The direct response to tropical heating in a baroclinic atmosphere. *J. Atmos. Sci.*, **52**,307-319

Jones, C., B. C. Weare, 1996: The role of low-level moisture convergence and ocean latent heat fluxes in the Madden and Julian oscillation: An observational analysis using ISCCP data and ECMWF analysis. *J. Climate,* **9**, 3086-3104.

Jones, C., 2000: Occurrence of extreme precipitation events in California and relationships with the Madden-Julian oscillation. *J. Climate,* **13**, 3576-3587.

Ju, J. H., and E. R. Zhao, 2005: Impacts of the low frequency oscillation in East Asia summer monsoon on the drought and flooding in the middle and lower valley of the Yangtze River. *J. Trop. meteorol*. **21**(2), 163-171. (In Chinese)

Kalney, E., and Coauthors, 1996: The NCEP/NCAR 40-year reanalysis project. *Bull. Amer. Meteor. Soc*., **77**, 437-471

Kessler, W. S., M. J. McPhaden, and K. M. Weickmann, 1995: Forcing of intraseasonal Kelvin waves in the equatorial Pacific,*J. Geophys. Res*., **100**, 10613–10631.

Knuston, T. R., K. M. Weickmann, 1987: 30-60 day atmospheric oscillation: composite life cyclones of convection and circulation anomalies, *Mon. Wea. Rev*., **115**, 1407-1436.

Lau, K. M., and P. H. Chan, 1985: Aspects of the 40–50 day oscillation during the northern summer as inferred from outgoing longwave radiation. *Mon. Wea. Rev.,* **114,** 1354-1367.

Lau, K. M., and S. Shen, 1988: On the dynamics of intraseasonal oscillations and ENSO, *J. Atmos. Sci*., **45**, 1781–1797.

Lawrence, D. M., and P. J. Webster, 2002: The boreal summer intraseasonal oscillation: Relationship between northward and eastward movement of

convection. *J. Atmos. Sci*., **59**, 1593-1606.

Li, C. Y., Z. X. Long., 2002: intraseasonal oscillation anomalies in the tropical atmosphere and Li Nino events, *Exchanges*, **7**, No.2, 12-15.

Li, C. Y., P. L. Wu, 1990: An observational study of 30-50 day atmospheric oscillation. Part 1: Structure and propagation, *Adv. Atmos. Sci.,* **7**, 294-304.

Li, C. Y., and Y. P. Zhou, 1994: Relationship between Intraseasonal oscillation in the tropical atmosphere and ENSO, *Chinese J. Geophysics*, **37**, 213-223 .

Madden, R. A., and P. R. Julian. 1971: Detection of a 40-50 day oscillation in the zonal wind in the tropical Pacific. *J. Atmos. Sci*., **28**, 702-708.

Madden, R. A., and P. R. Julian, 1972: Description of global scale circulation cells in the tropics with 40-50 day period. *J. Atmos. Sci*., **29,** 1109-1123.

Madden R. A, and P. R. Julian.1994: Observations of the 40-50-day tropical oscillation-A review. *Mon.Wea. Rev.*, **122:**814-837.

Maloney, E. D., D. L. Hartmann, 1998: Frictional moisture convergence in a composite life cycle of the Madden-Julian oscillation. *J. Climate*., **11**,2387-2403

Maloney, E. D., and D. L. Hartmann. 2000: Modulation of eastern North Pacific hurricanes by the Madden-Julian oscillation. *J. Climate*, **13**, 1451–1460.

Matthews, A. J. 2000: Propagating mechanisms for the Madden-Julian Oscillation. *Q. J. R. Meteorol. Soc*., **126,** 2637-2651.

Mu, M. Q., and C. Y. Li, 2000: The onset of summer monsoon over the South China Sea in 1998 and action of atmospheric intraseasonal oscillation. *Climate and Environmental Research*, **5**, 375-387 (in Chinese).

Paegle, J. N, L. A. Byerle, and K. C. Mo, 2000: Intraseasonal modulation of South American summer precipitation. *Mon. Wea. Rev*., **128**, 837–850.

Rui, H., and B. Wang, 1990: Development characteristics and dynamic structure of tropical intraseasonal convection anomalies. *J. Atmos. Sci.,*. **47**, 357–379.

Sperber, K. R. 2004: Propagation and the vertical structure of the Madden-Julian Oscillation. *Mon.Wea.Rev.*, **131**, 3018-3037.

Ting, M., and P. D. Sardeshmukh, 1993: Factors determining the extratropical

response to equatorial diabatic heating anomalies. *J. Atmos. Sci*., **50**,907-918.

Wang, L., and Coauthors, 2008: Analysis of the severe cold Surge, ice-snow and frozen disasters in South China during January 2008: I. Climatic features and its impacts. *Meteorological Monthly*, **34**(4): 95－100 (in Chinese)

Wheeler, M. C., and H. H. Hendon, 2004: An all-season real-time multivariate MJO Index: Development of an index for monitoring and prediction. *Mon. Wea. Rev*., **132**, 1917-1932.

Wheeler, M. C., H. H. Hendon, C. Sam, M. Holger, D. Alexis, 2009: Impacts of the Madden-Julian Oscillation on Australian Rainfall and circulation. *J. Climate*. **22**(6), 1482-1498.

Wheeler, M. C., and J. L. McBride, 2005: Australian-Indonesian monsoon. *Intraseasonal variability in the Atmosphere Ocean Climate System*. Praxis, Springer, 125-173.

Wilks, D. S., 2006: *Statistical Methods in the Atmospheric Sciences*. Academic Press, 648 pp.

Woolnough, S. J., J. M. Slingo, B. J. Hoskins, 2000: The relationship between convection and sea surface temperature on intraseasonal timescales. *J. Climate*, **13**, 2086-2104.

Xu, G. Q., Q. G. Zhu, J. S. Xue, and J. H. He, 2004: A pilot study of propagation mechanism of precipitation low-frequency variation over China in 1998. *J. Atmos. Sci.,* **28**(5), 736-746. (In Chinese)

Yang, H., and C. Y. Li, 2003: The relation between atmospheric intraseasonal oscillation and summer severe flood and drought in Changjiang-Huaihe river basin. *Adv. Atmos. Sci.*, **20**(4), 540-553.

Yeo, I. K., and R. A. Johnson, 2000: A new family of power transformation to improve normality or symmetry. *Biometrika*, **87**, 954–959.

Zhang, L. N., B. Z. Wang, Q. C. Zeng, 2009: Impacts of the Madden-Julian Oscillation on Summer Rainfall in Southeast China. *J. Climate*, **22**,201-216.

Zhang, C., 2005: Madden–Julian oscillation. *Reviews of Geophysics,* **43**, 1–36.

Zhang, C., and J. Gottschalck, 2002: SST anomalies of ENSO and the Madden-Julian

Oscillation in the equatorial Pacific, *J. Climate*, **15**, 2429–2445.

List of the figures

Fig. 1. Phase space represented by the two-component MJO index (RMM1, RMM2) designed by Wheeler and Hendon (2004). Eight defined regions of the phase space are labeled, as is the region considered to signify weak MJO activity. Also labeled are the approximate locations of the enhanced convective signal of the MJO for that location of the phase space, e.g. the ‘‘Indian Ocean’’ for phases 2 and 3.

Fig. 2. Locations of 545 meteorological stations in China.

Fig. 3. Standard deviation of daily rainfall in China during winter (Dec－Feb) for 1971－2000 (units: mm).

Fig. 4. Composites of daily rainfall anomalies for the eight MJO phases (contour interval is 0.3 mm d^{-1}; shading indicates where significance exceeds the 5% confidence level).

Fig. 5. As in Fig. 4, except for rain day anomalies (contour interval is 2 days; shading indicates significance exceeding the 5% confidence level).

Fig. 6. Composite regional mean (longitude $\geqslant$ 105°E, latitude $\leqslant$ 32.5°N) rainfall anomalies (bar; mm d^{-1}) and percentage of rainfall anomalies (line; %) for eastern China for the eight MJO phases.

Fig. 7. Composite anomalies of moisture flux integrated from 1000–300 hPa (vector; kg m^{-1} s^{-1}; vectors are plotted only where they are locally significant at the 95% confidence level) and moisture flux divergence (contour interval is $20\times x10^{6}$g s^{-1} m^{-2}; shading indicates where significance exceeds the 95% confidence level; negative (positive) values indicate the moisture convergence (divergence)) for the eight MJO

phases.

Fig. 8. Geopotential height anomalies of the southern trough of the Bay of Bengal (15—25^{0}N, 85–95^{0}E, line, left axis) for the eight MJO phases(the bar indicates the value (right axis) that the *t*-test value minus which at 95% confidence level; therefore, a positive value indicates the composite for the corresponding MJO phase exceeding the 95% confidence level).

Fig. 9. Composite 5870 gpm contours at 500 hPa for MJO phase 2 (solid line) and phase 6 (dashed line).

Fig. 10. Composites of 500 hPa geopotential height anomalies for the eight MJO phases (contour interval is 5 gpm; solid (dashed) lines indicate positive (negative) anomalies; shading indicates where significance exceeds the 5% confidence level).

Fig. 11. Geopotential height anomalies of the low trough over Central Asia (30–40°N, 65–75°E; line; left axis) for the eight MJO phases (the bar indicates the value (right axis) that the *t*-test value minus which at 95% confidence level; therefore, a positive value indicates the composite for each MJO phase exceeding the 95% confidence level).

Fig. 12. Composites of SLP anomalies (contour interval is 0.5 hPa; shading indicates where significance exceeds the 5% confidence level) and 850 hPa wind anomalies (m s^{-1}; vectors are plotted only where they are locally significant at the 95% confidence level) for the eight MJO phases.

Fig. 13. East Asian winter monsoon index (line; left axis) for the eight MJO phases. A positive (negative) value indicates southerly (northerly) anomalies and weak (strong) East Asian winter monsoon (the bar indicates the value (right axis) that the *t*-test value minus which at 5% confidence level; therefore, a positive value indicates the

composite for each MJO phase exceeding the 95% confidence level).

Fig. 14. Vertical velocity anomalies (contour interval is 0.5 hPa s^{-1}; shading indicates where significance exceeds the 5% confidence level) and meridional-vertical wind vectors (vectors are plotted only where they are locally significant at the 5% confidence level) averaged between 110–120°E for the eight MJO phases.

All figures

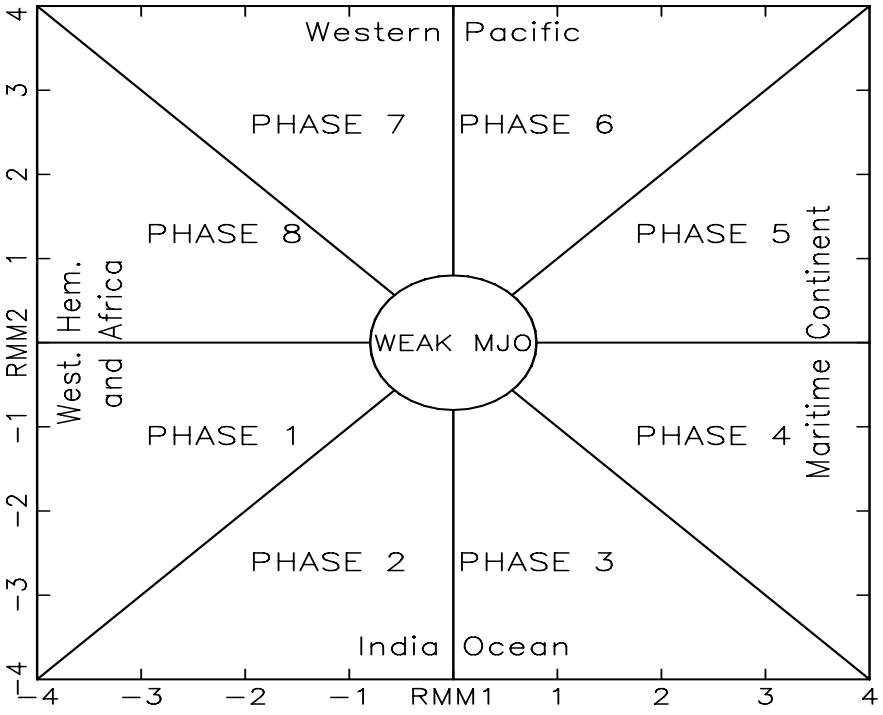

Fig.1 Phase space represented by the 2-component MJO index (RMM1, RMM2). (Designed by Wheeler and Hendon, 2004) Eight defined regions of the phase space are labeled, as is the region considered to signify weak MJO activity. Also labeled are the approximate locations of the enhanced convective signal of the MJO for that location of the phase space, e.g., the ‘‘Indian Ocean’’ for phases 2 and 3.

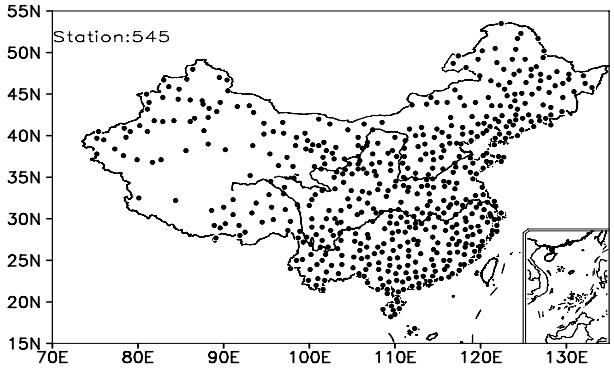

Fig.2 Locations of 545 meteorological stations in China

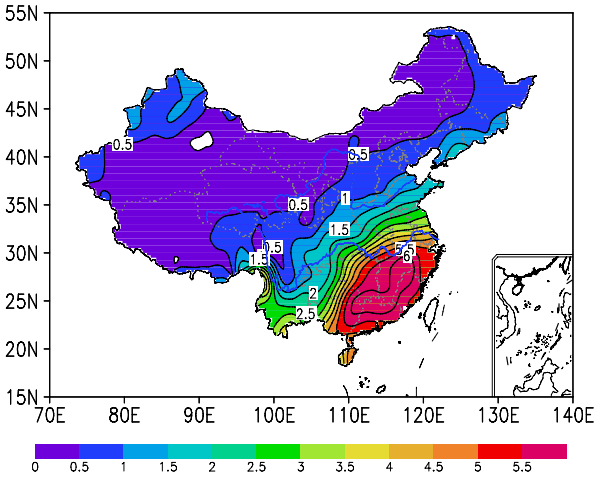

Fig.3 Standard deviation of daily rainfall in China during winter (Dec-Feb) for 1971-2000 (mm)

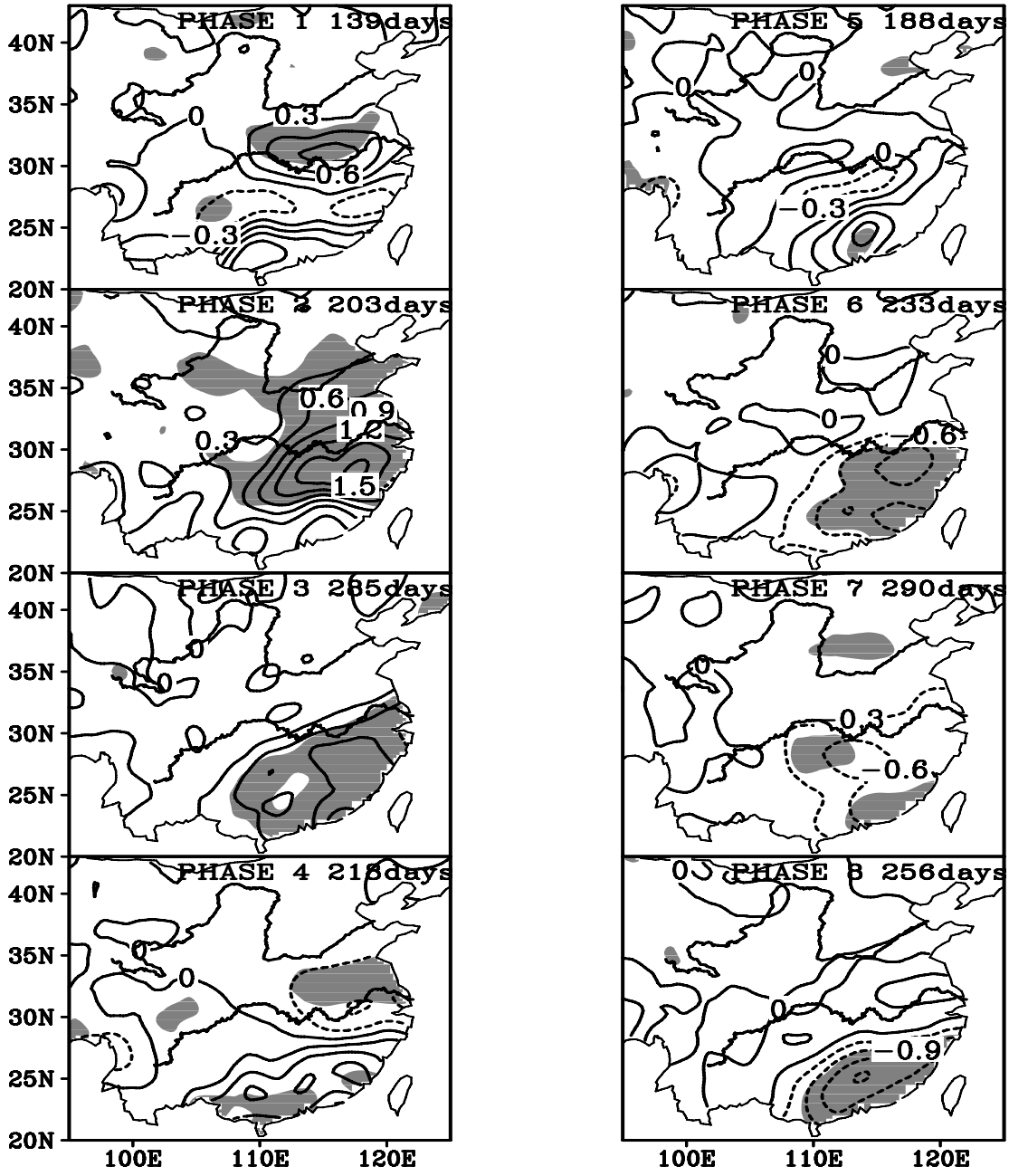

Fig.4 Composites of daily rainfall anomalies for 8 MJO phases (contour interval is 0.3mm d^{-1}; Shaded indicates where significant test exceeds 95% confidence level).

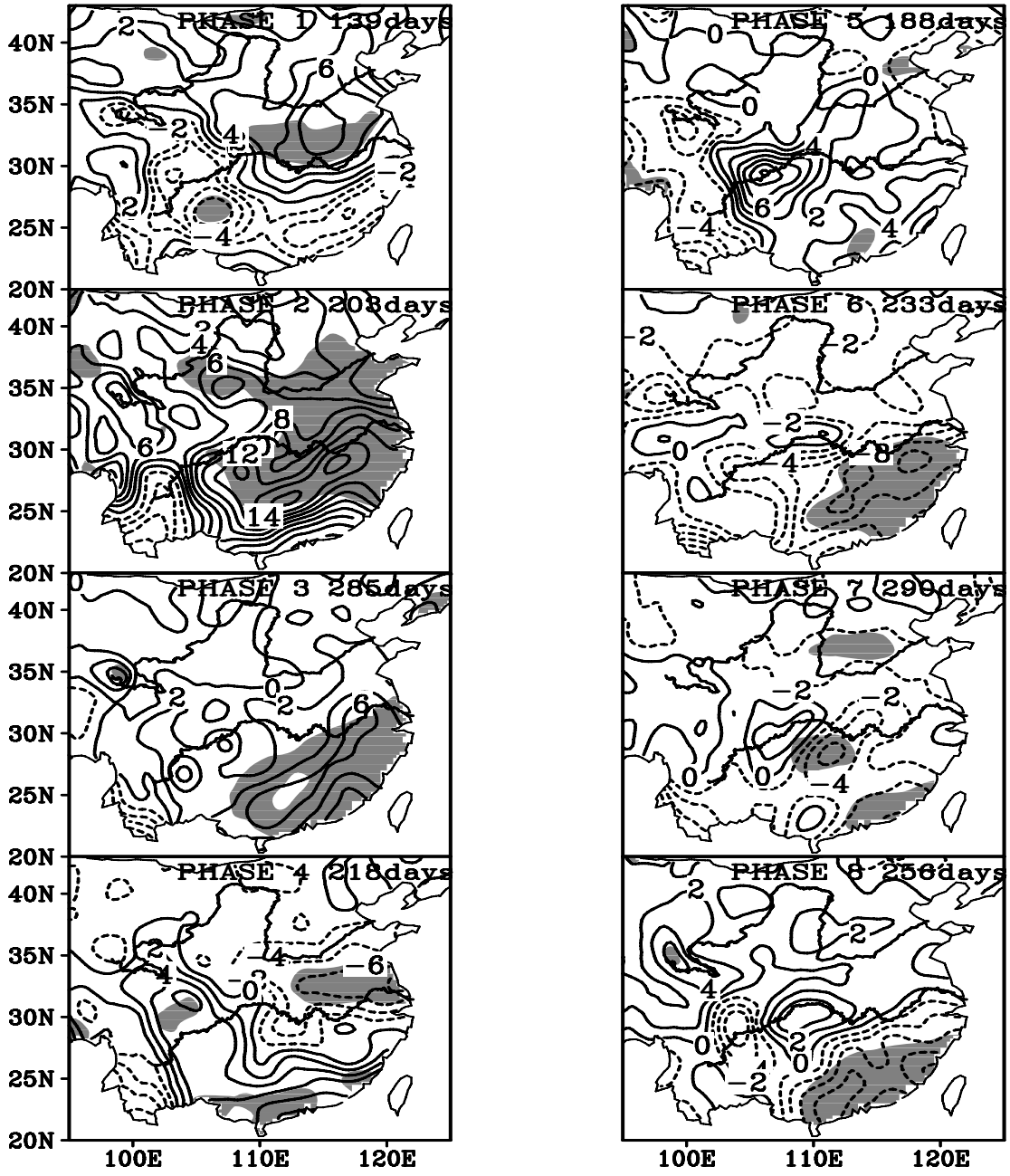

Fig.5. As in Fig.4, except for rain day anomalies (contour interval is 2days; Shaded indicates where significant test exceeds 95% confidence level).

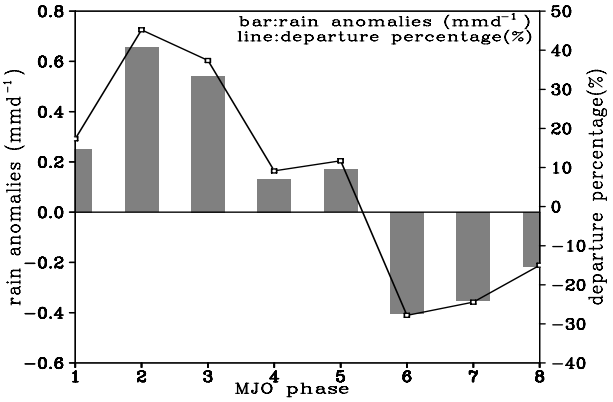

Fig.6 Composites regional mean (longitude≥105°E, and latitude≤32.5°N) rainfall anomalies (bar, mm d^{-1}) and percentage of rainfall anomalies (%, line) of Eastern China for 8 MJO phases.

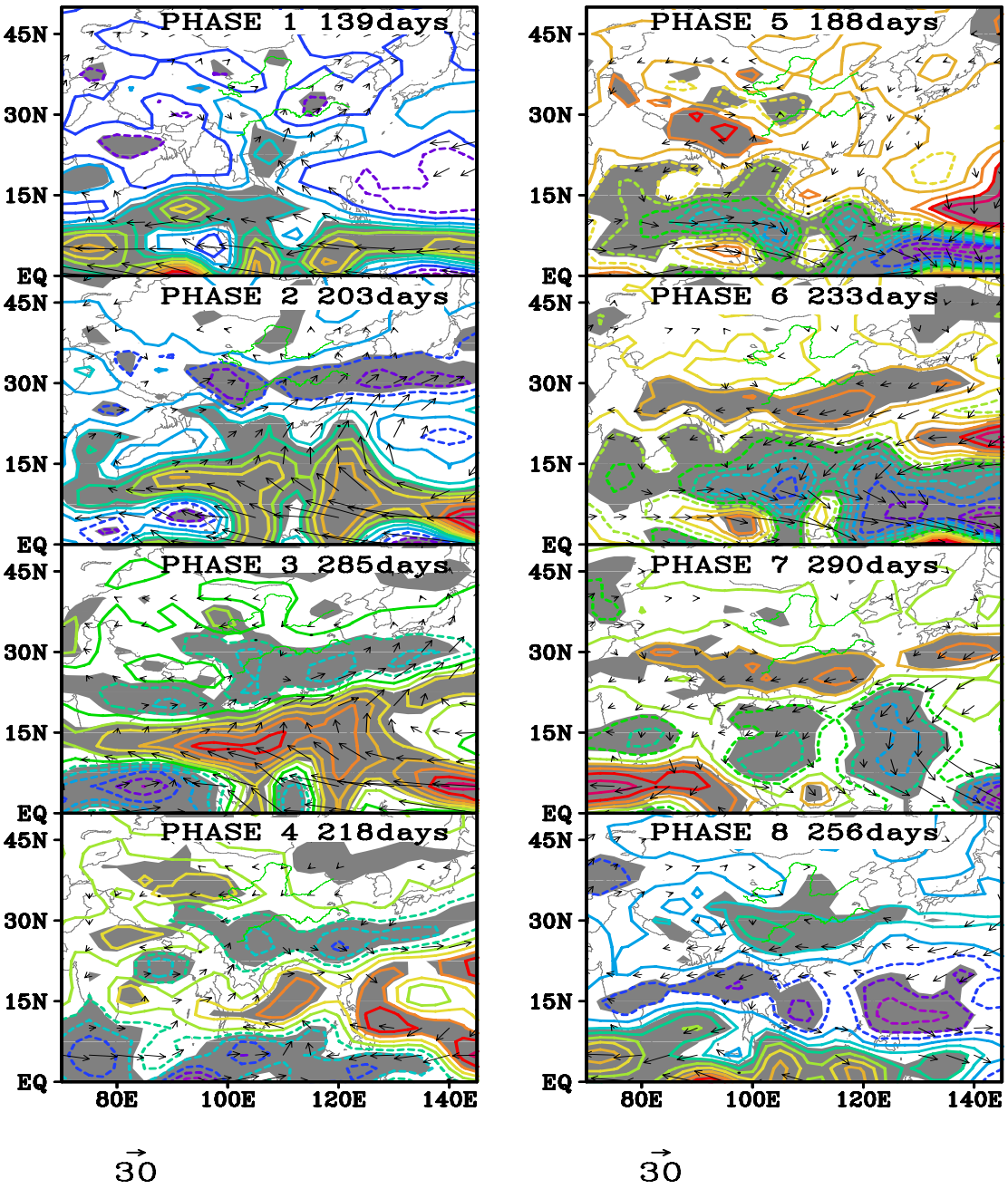

Fig.7 Composites anomalies of moisture flux integrate from 1000 hPa to 300 hPa (vector, kg m^{-1} s^{-1}, vectors are plotted only where they are locally significant at the 95% confidence level.) and moisture flux divergence {contour interval is $20x10^{6}$g s^{-1} m^{-2}; Shaded indicates where significant test exceeds 95% confidence level; Negative (positive) values indicate the moisture convergence (divergence)} for 8 MJO phases

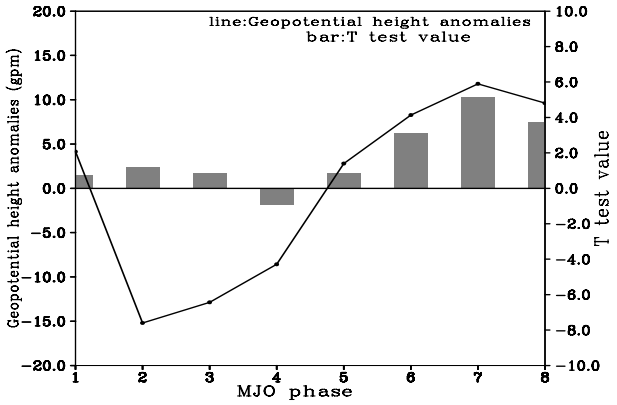

Fig.8 Geopotential height anomalies of the southern trough of the Bay of Bengal (15°N-25°N, 85 °E-95°E, line, left axis) for 8 MJO phases. {The bar indicates the value(right axis) that T test value minus which at 95% confidence level, therefore, positive value indicates the composite for corresponding MJO phase exceeds 95% confidence level.}

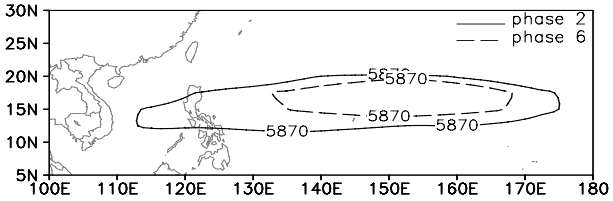

Fig.9 Composites 5870 gpm contour at 500 hPa for MJO phase 2 (solid line) and phase 6 (dashed line)

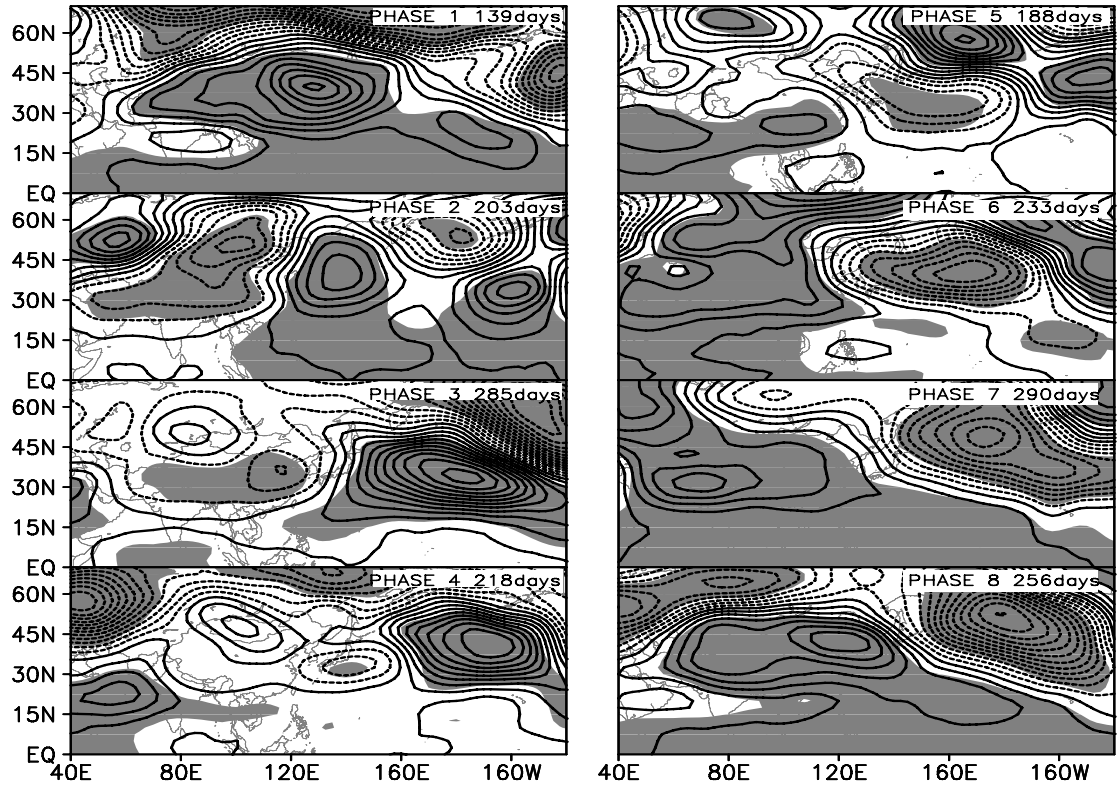

Fig.10 Composites of 500 hPa geopotential height anomalies for 8 MJO phases {Contour interval is 5 gpm; Solid (dashed) lines indicate positive (negative) anomalies; Shaded indicates where significant test exceeds 95% confidence level}.

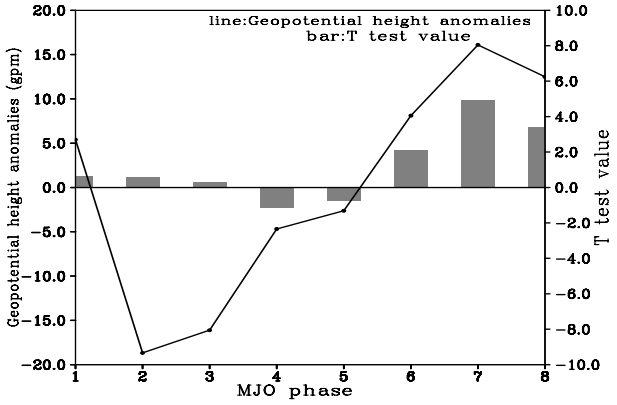

Fig.11 Geopotential height anomalies of the low trough over Central Asia (30°N-40°N, 65°E-75°E; line; left axis) for 8 MJO phases. {The bar indicates the value(right axis) that T test value minus which at 95% level, therefore, positive value indicates the composite for each MJO phase exceeds 95% confidence level}

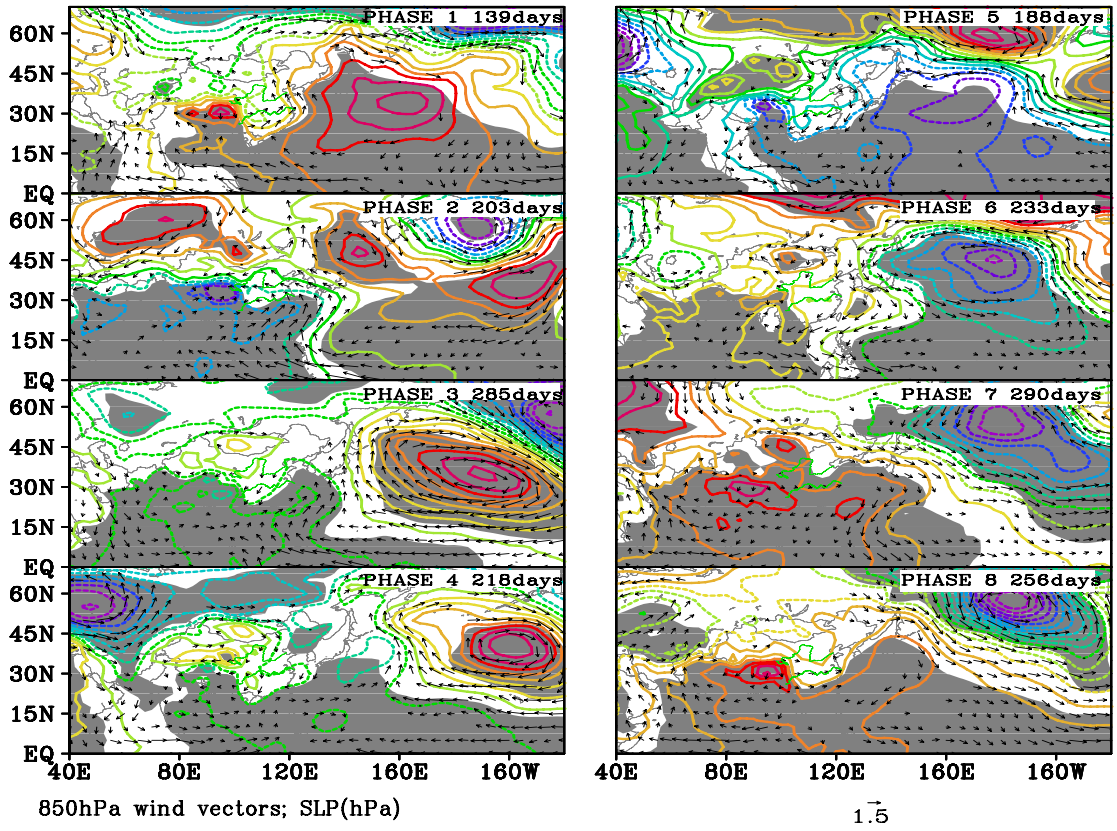

Fig.12 Composites of SLP anomalies (contour interval is 0.5hPa, Shaded indicates where significant test exceeds 95% confidence level) and 850 hPa wind anomalies (m s^{-1}, Vectors are plotted only where they are locally significant at the 95% confidence level.) for 8 MJO phases.

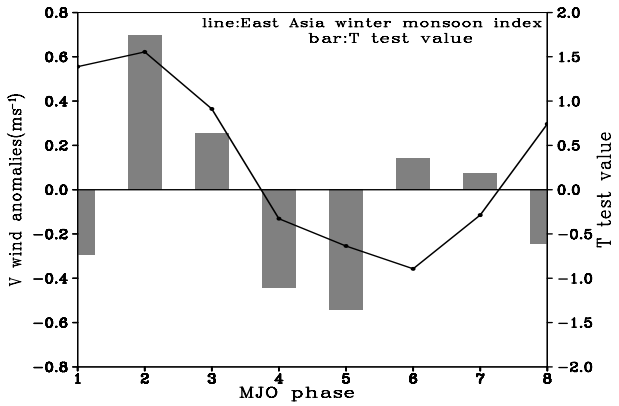

Fig.13 East Asia winter monsoon index (line, left axis) for 8 MJO phases. The positive value (negative) indicates the southerly (northerly) anomalies and weak (strong) East Asia winter monsoon. {The bar indicates the value(right axis) that T test value minus which at 95% level, therefore, positive value indicates the composite for each MJO phase exceeds 95% confidence level}

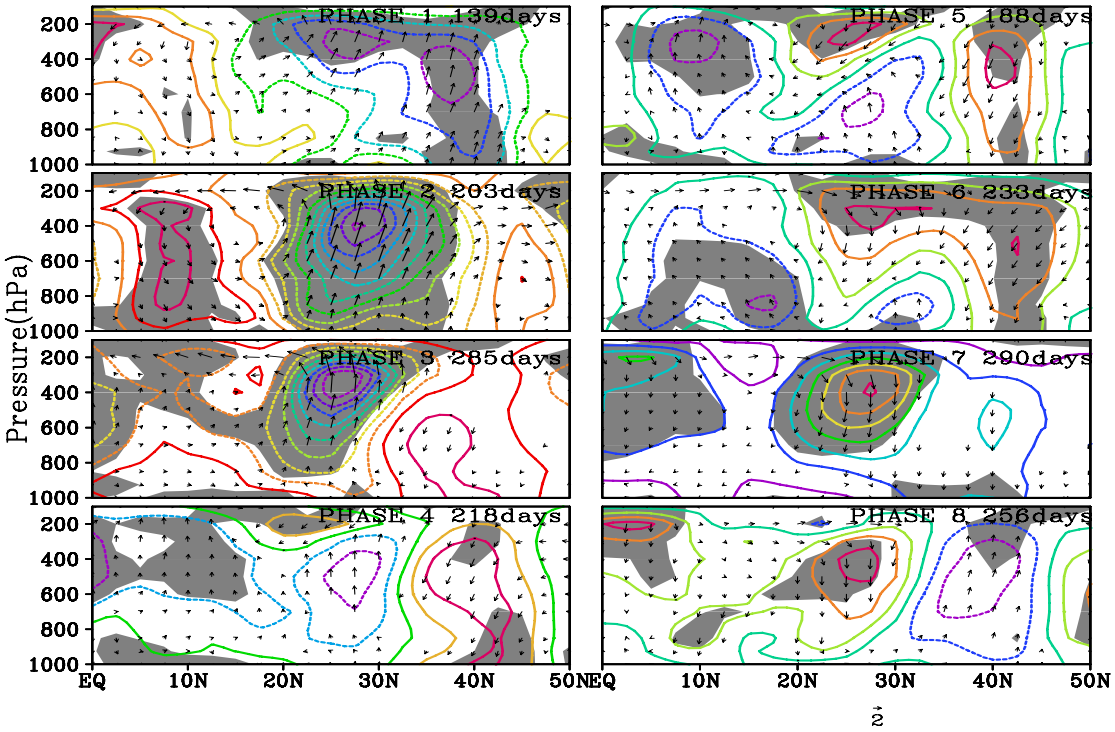

Fig.14 Vertical velocity anomalies (contour interval is 0.5 hPa s^{-1}, Shaded indicates where significant test exceeds 95% confidence level) and meridional-vertical wind vectors (Vectors are plotted only where they are locally significant at the 95% confidence level) averaged between 110°-120°E for 8 MJO phases.